

PRACTICAL ASPECTS OF ROTOR AERODYNAMIC AND AEROACOUSTIC DESIGN OPTIMIZATION

Witold Klimczyk

Łukasiewicz Research Network – Institute of Aviation, Warsaw, Poland

Abstract

Selected aspects of aerodynamic and aeroacoustic rotor design optimization are presented in this work. With the focus on practical aspects of rotor optimization, the discussion covers the selection of computational modeling methods, definition of parametric model, and formulation of the optimization problem. The work presents three distinct aeroacoustic rotor optimization case studies. Firstly, an analysis of a spline-based parametric model is performed by varying the number of knots used to define radial distributions of chord and twist. Global sensitivity analysis is performed to establish the effect of the number of parameters on the individual parameter importance and results. Secondly, a small-scale rotor optimization is performed using computational tools for the tonal and broadband noise components. The influence of noise metric is presented by comparing the difference between sound pressure level with its A-weighted variation. The last case study presents a variable-pitch prop-rotor design. It utilizes a multi-fidelity optimization framework in a multi-point optimization study with four objective functions. The work is focused on addressing aspects commonly omitted in the literature.

Keywords: rotor optimization, UAV, AAM, aerodynamics, aeroacoustics

1. Introduction

The use of optimization methods to design lifting surfaces is an area of significant focus for a few decades now. This stems from the significance of aerodynamic efficiency on the overall vehicle performance on the one hand, and the efficiency of algorithms coupled with computational models, operating without human interaction on the other.

In recent years, the technological advancements resulted in the emergence of the Advanced Air Mobility (AAM) sector. AAM encompasses air vehicles of various scales, types, and intended uses. Electric or hybrid-electric propulsion is typically utilized for a range of different vehicles, including multirotors as well as fixed- and tilt-wing aircraft [1]. AAM rotors are diverse, ranging from small, low-Reynolds number UAV propellers, up to large-scale variable-pitch rotors used for both vertical take-off and high-speed forward flight. The aerodynamic design of AAM rotors is closely related to their noise signature, particularly important in urban and other densely-populated areas. Therefore, the aeroacoustic analysis of rotors has been adopted in many recent studies [2].

1.1 Current practices

Rotor aeroacoustic optimization is relatively common in the literature. Several recent works are briefly summarized here, which are intended to provide an overview of common approaches in aeroacoustic rotor design.

A multi-objective optimization of Micro Air Vehicle (MAV) rotors was performed using Non-Linear Vortex Lattice method [3]. The optimization process of 10 design variables defining blade planform was carried out using an evolutionary algorithm directly calling the computational model. Higher-fidelity URANS-based surrogate modeling-driven rotor optimization was performed [4]. In this work

the acoustic pressure peak at a single observer location was employed for the objective function. Rotor parameters described blade planform and airfoil. No assessment of the individual parameters influence on the objective function was performed, although a comparison of the baseline and optimized airfoils revealed a noticeable acoustic pressure difference.
A multi-point (hover-cruise) UAM-class prop-rotor optimization was carried out using a blade element model coupled with a vortex wake model and an Amiet's model based method for the turbulent boundary layer-trailing edge noise [5]. The blade geometry was defined using elliptic functions. The multi-objective optimization problem was reduced to single objective by a weighted objective function approach.
Another example of rotor planform optimization based on URANS simulations in a surrogate-driven framework was performed for a quadrotor in forward flight [6]. This study highlighted the influence of the acoustic metric, showing that the use of A-weighted sound pressure level (SPL) instead of the raw SPL can be used to report substantial noise reductions.
Some insight into the selection of geometric parameters was performed in BEMT-based 1.5 m diameter cruise propeller optimization [7]. The influence of a subsequently tightened acoustic constraint on the chord and twist radial distributions was shown. Although the influence of planform parameters was not quantified, the results provide a valuable intuition in their selection.
A more detailed study involving not only aerodynamic and aeroacoustic, but also structural analysis was performed using a BEMT model [8]. The study included both acoustic and structural constraints to determine aerodynamically optimum propellers. It confirmed the domination of rotational speed on the acoustic performance, however, the relative importance of planform parameters remains unknown.
In this work, following aspects are discussed in relation to the aerodynamic and aeroacoustic AAM rotor optimization:

- The definition of blade parametric model. Parameters sensitivity assessment is typically not reported in the literature. As a consequence, the selection of unimportant variables is replicated in subsequent studies. For example, practical examples show, that chord distribution has a limited impact on the aerodynamic and aeroacoustic performance of a rotor, compared to the impact of twist [9, 10].
- The importance of the aeroacoustic metric on the optimization results. Even though it is a well-known aspect in the aeroacoustic community, there is common lack of understanding the noise complexity.
- The selection of the optimization framework and computational models.

Section 2 describes the general formulation of the optimization problem in a rotor optimization context. Section 3 provides case studies of aeroacoustic rotor design, showing the importance of the optimization problem formulation in a realistic rotor design approach.

2. Rotor Aeroacoustic Optimization

A multi-objective optimization problem can be formulated as the minimization of the objective functions $f(\mathbf{x})$, subject to a set of inequality (g) and equality (h) constraints:

$$\begin{aligned} \underset{\mathbf{x}}{\text{minimize}} \quad & f_i(\mathbf{x}), \quad i = 1,\ldots,m \\ \text{subject to} \quad & g_j(\mathbf{x}) \leq 0, \quad j = 1,\ldots,n, \\ & h_k(\mathbf{x}) = 0, \quad k = 1,\ldots,o, \\ & \mathbf{l} \leq \mathbf{x} \leq \mathbf{u} \end{aligned}$$

where $\mathbf{x}$ denotes the vector of design variables bounded between $\mathbf{l}$ and $\mathbf{u}$. This formulation highlights the complexity of real-world optimization problems:

1. Multiple objectives, such as the minimization of power consumption and noise emissions in propeller design requires calculation of aerodynamic efficiency and a noise-related merit function.

2. Multiple disciplines. While an aeroacoustic optimization of a propeller is a multi-disciplinary problem, it can be directly reformulated to multi-objective one. In contrast, an aerostructural design involving aerodynamic efficiency and structural design does not necessarily lead to multiple objectives, but rather imposes constraints and increases problem complexity.

3. Multiple operating points, which are used to ensure the design is optimal on the mission level, rather than solely in a single phase. In the context of tilt-rotor/wing aircraft, multi-point design involves designing propeller for hover and cruise, which are characterized by significantly different requirements and operating conditions.

An aeroacoustic rotor optimization problem formulation is briefly summarized in the following subsections, covering the aspects of objective function definition, computational model selection and the optimization framework. The formulation of aeroacoustic optimization problem is typically an iterative process, where all aforementioned aspects influence each other and require the selection of consistent methods.

2.1 Objective function

Rotor aeroacoustic optimization is concerned with objective functions covering two disciplines. The objective function specifying aerodynamic merit is relatively straightforward, as it typically refers to the minimization of power (or similar metric). On the other hand, the aeroacoustic merit function can be defined in multiple ways. The relative performance of the solutions is highly dependent on its definition. The main reasons for this complexity are:

- The noise characteristics are captured in the frequency domain. Typically, SPL is used as a metric which provides a simple measure of the noise level. However, if noise perceived by human ear is analyzed, a frequency-based weighting is often applied. Regardless of the selected merit function, the use of a single noise measure is a simplification.

- The noise source exhibits strong directivity, leading to non-uniform sound distribution across observation points. Isolated rotor directivity varies only with the elevation angle, however, a realistic propulsor characterized by aerodynamic and acoustic interactions results in highly non-uniform noise patterns, also in the azimuthal direction.

2.2 Computational model

A variety of computational models has been applied in aeroacoustic optimization of rotors. The most popular selections, in the order of increasing computational cost, are: BEMT, Non-Linear Vortex Lattice, free-wake methods (Vortex Particle Method), steady RANS and URANS. The use of higher-fidelity methods is not feasible, due to the computational cost, even if efficient optimization using surrogate models or adjoint methods are used. The use of cheap, low-fidelity methods is preferred at early design stages, whereas a detailed design often requires the use of blade geometry-resolved CFD.

2.3 Optimization framework

Optimization frameworks are commonly divided into gradient-based and gradient-free methods. Gradient-based methods require a starting point and iteratively proceed to the local optimum by following the path determined using gradients. Gradient-based methods became very popular in CFD-based optimization due to the efficient gradient calculation using adjoint. Gradient-free methods are typically global, do not require a starting point but rather a bounded design space. They are often based on evolutionary heuristics and incorporate population-based search, which eventually leads to a global optimum. Evolutionary algorithms are often used together with surrogate modeling methods, which build the objective function approximation based on limited input data. Surrogate-based optimization is commonly used in CFD-based optimization. The selection of framework depends, among others, on the available computational models, budget and problem requirements.

3. Case studies

3.1 Small-scale rotor design

The first case study presented in this work is focused on the definition of the rotor parametric model. The parametric model is based on the spline-based definition of chord and twist radial distributions. The number of knots used to define each spline must be selected carefully. The number of design variables influences the cost of optimization. On the other hand, insufficient model flexibility may not allow to reach a satisfactory design. Figures 1 and 2 present example of spline-based parameterization applied to chord and twist radial distributions, respectively. The knots are positioned in equal distances along the radius. The market APC12x5.5 propeller geometry was used as a reference, from which the lower and upper bounds of knots positions were determined. Effects of increasing the number of variables from three to seven are clearly visible. With three parameters, the radial distributions are similar in shape, and there is some flexibility in collective chord and twist. Subsequent addition of knots adds a lot of flexibility, in particular to the local features. With seven knots, the randomly generated splines exhibit non-monotonic behavior, allowing exotic shapes not feasible in practical applications.

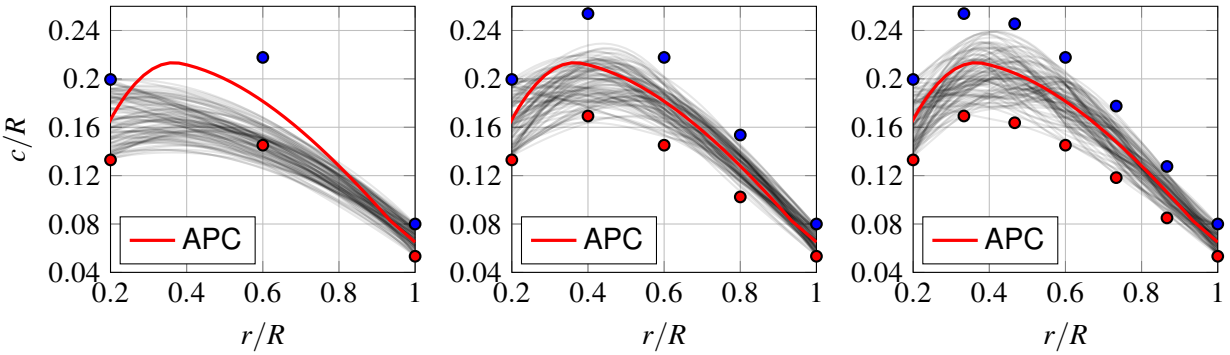


Figure 1 – Chord distributions of a sample of 100 design points parameterized with three (left), five (middle) and seven (right) knots. Upper (blue) and lower (red) knot position bounds are presented.

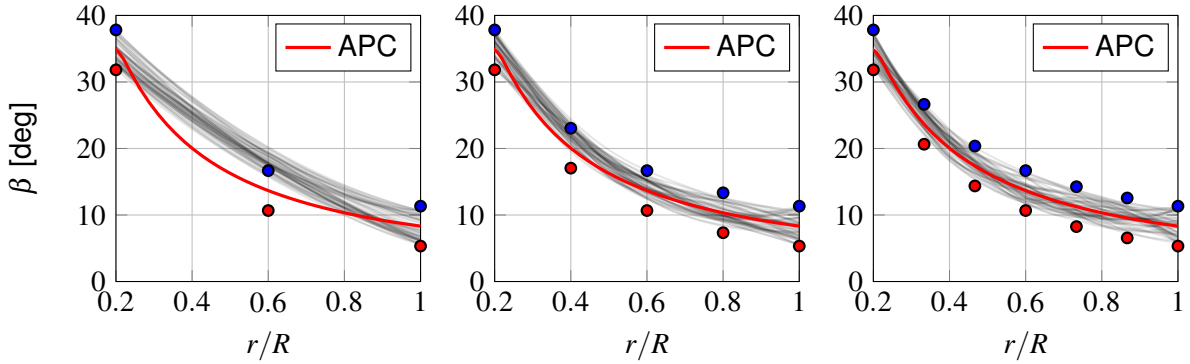


Figure 2 – Twist distributions of a sample of 100 design points (every second was shown here) parameterized with three (left), five (middle) and seven (right) knots. Upper (blue) and lower (red) knot position bounds are presented.

Figure 3 presents Sobol' indices for the presented parametric models. Sobol' index value indicates the variance of thrust associated with the variance of individual parameters defining knots positions of chord and twist distributions, as well as the rotational speed. This metric is a useful tool in assessing the relative importance of parameters on the output of interest. Additionally, the method of variance decomposition provides information regarding interactions between parameters. As expected, the importance of individual parameters defining the blade geometry decreases as the number of knots increases. This is a consequence of increasingly local scope of every knot. The most significant knots are in the mid-outer part of the blade, both for chord and twist distributions. Interestingly, for the

case with the least parameters, chords are more significant than twist, which changes as the number of knots increases. Moreover, the significance of rotational speed also increases with increasing number of knots.

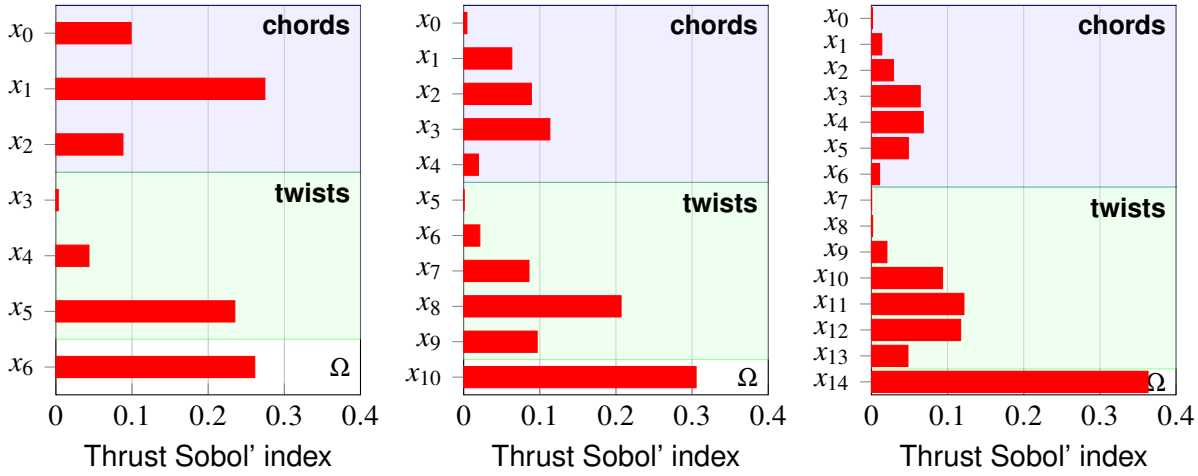


Figure 3 – Thrust Sobol' indices for 7 (left), 11 (middle) and 15 (right) parameters.

A similar plot in Figure 4 presents Sobol' indices for the SPL. The sensitivity study indicates a more pronounced domination of the rotational speed importance compared to the thrust sensitivity. This is a consequence of SPL scaling with both thrust (loading noise) and speed (thickness noise). The relative importance of input parameters on torque and power is similar. Consequently, decisions on the selection of the input parameters can be performed. Parameters with Sobol' index value close to zero can be removed from the optimization process (fixed to a selected value). Parameters with low Sobol' index can be redefined, for example by extending their bounds. Finally, parameters with high Sobol' index dominate the search, which in same cases can hamper the search. Strategies include splitting such variables into two (or more), or tightening their bounds.

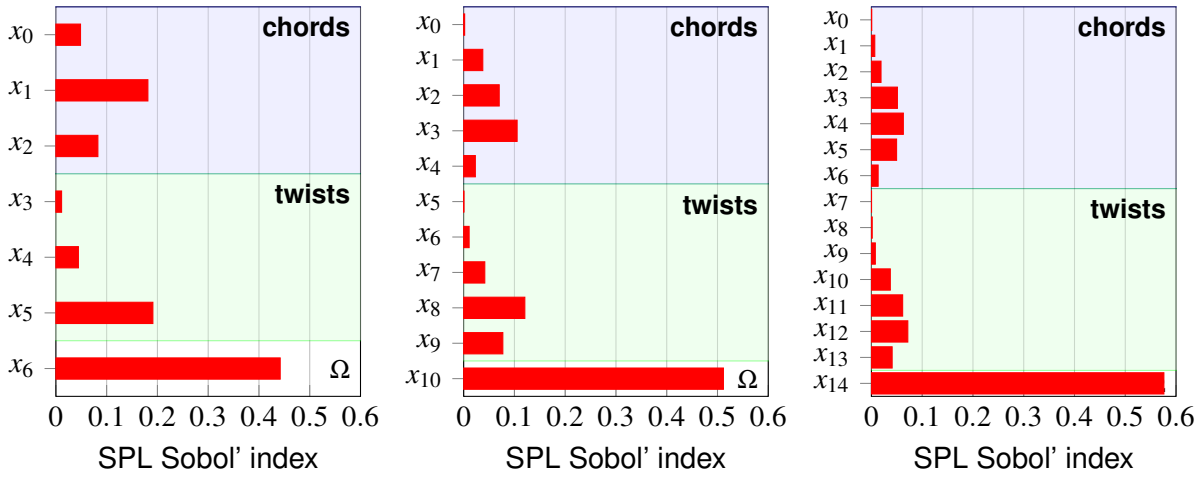


Figure 4 – SPL Sobol' indices for 7 (left), 11 (middle) and 15 (right) parameters.

Three optimization processes using 7, 11 and 15 parameters were carried out according to the following problem statement:

$$\begin{aligned} \underset{\mathbf{x}}{\text{minimize}} \quad & P(\mathbf{x}), \mathrm{SPL}(\mathbf{x}) \\ \text{subject to} \quad & T_{\text{req}} - 10 \leq 0, \\ & \mathbf{l} \leq \mathbf{x} \leq \mathbf{u} \end{aligned}$$

Here, a multi-objective problem seeks a solution minimizing power P and SPL, subject to a constraint $T \geq 10\,\text{N}$. Figure 5 presents results in the form of the last populations of the NSGAII search. All

presented design points satisfy the thrust constraint. It can be observed that increasing the number of variables shifts the Pareto front towards more optimal solutions. At the same time, the variation of SPL is negligilbe, while the power variation remains relatively small. There is no clear distinction between aerodynamic and aeroacoustic optima.

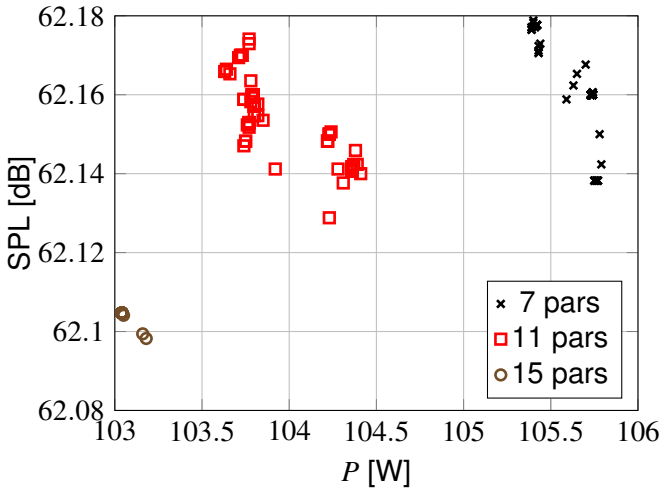


Figure 5 – Power-SPL Pareto fronts obtained from optimization performed using 7, 11 and 15 parameters.

3.2 Micro Air Vehicle rotor design

Micro Air Vehicle (MAV) aeroacoustic rotor design is an interesting case study due to the high relative importance of the broadband noise component. The optimization process was inspired by the mini UAVs, with the total weight ranging from 1 to 2 kg spread between four propellers of 10 cm radius. The typical operating condition of MAV is hover. Apart from the minimization of SPL, separate objective functions were defined for the tonal and broadband components. Aerodynamic performance optimization was defined by minimization of $-$FM. The resulting optimization problem is formulated in the following way:

$$\begin{aligned} \underset{\mathbf{x}}{\text{minimize}} \quad & -\mathrm{FM}(\mathbf{x}), \mathrm{SPL}(\mathbf{x}), \mathrm{SPL}_{\mathrm{tonal}}(\mathbf{x}), \mathrm{SPL}_{\mathrm{broadband}}(\mathbf{x}) \\ \text{subject to} \quad & T_{\mathrm{req}} - T \leq 0, \\ & \mathbf{l} \leq \mathbf{x} \leq \mathbf{u} \end{aligned}$$

where T_{req} is used to ensure design robustness by using two values, i.e. $T_{\mathrm{req}} = 3\,\mathrm{N}$ and $4\,\mathrm{N}$. It should be noted, that unless an additional treatment of this constraint is applied, the problem takes the form of optimization of eight objective functions (four for each value of T_{req}) or is divided into two separate processes.

In this study, the aerodynamic model was computed using a steady RANS model of a single blade in hover using Ansys Fluent. The tonal noise component was determined using F1A formulation based on the RANS solution [12]. The broadband noise component was determined based on the low-fidelity airfoil trailing edge noise model BPM [13] using NAFNoise [14].

The parametric model consists of 12 parameters. Chord and twist radial distributions were parameterized using splines, with knots positions at fixed radial positions used as design variables. A single sweep parameter was used to apply swept tip, starting from $r/R = 0.7$. Two parameters were used to define airfoil camber at the root and tip of the blade. Lastly, rotational speed was allowed to vary between 7000 and 9000 RPM. The bounds very determined based on BEMT analysis to ensure optimum coverage of the required search space, i.e. the possibility to achieve required thrust at all rotational speeds.

3.2.1 Initial sample analysis

The optimization process followed an adaptive surrogate-based framework with infills based on the objective function and maximum improvement criteria. The initial sample of 120 points is presented in Figure 6. It can be observed, that for the whole rotational speed range the thrust of 3 N and 4 N can be obtained. Additionally, thrust was plotted against the mid-span twist parameter (x6) and the tip airfoil camber (x10). A small positive correlation is observed. Figure 7 presents the same input parameters influence on FM. While the parameters x6 and x10 show marginal correlation, the rotational speed seems to be uncorrelated.

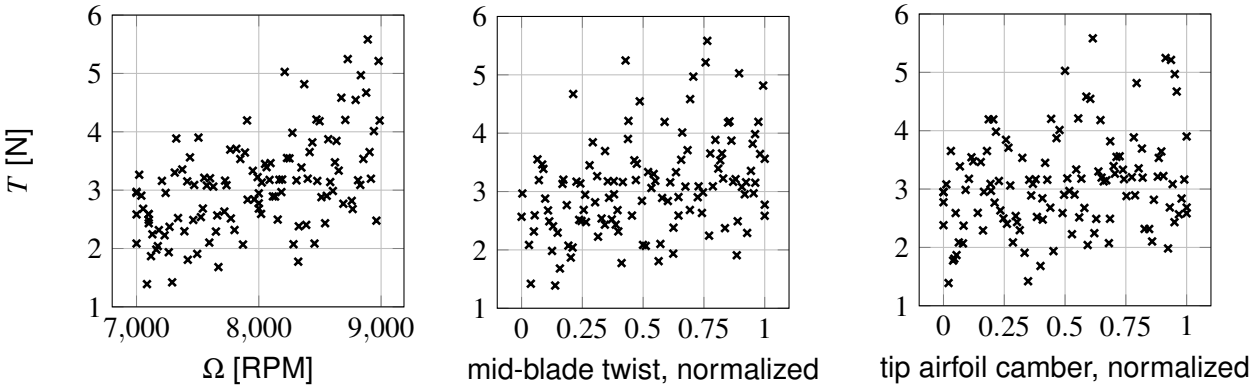


Figure 6 – Thrust plotted against selected input parameters: rotational speed (left), mid-blade twist (middle) and tip airfoil camber (right).

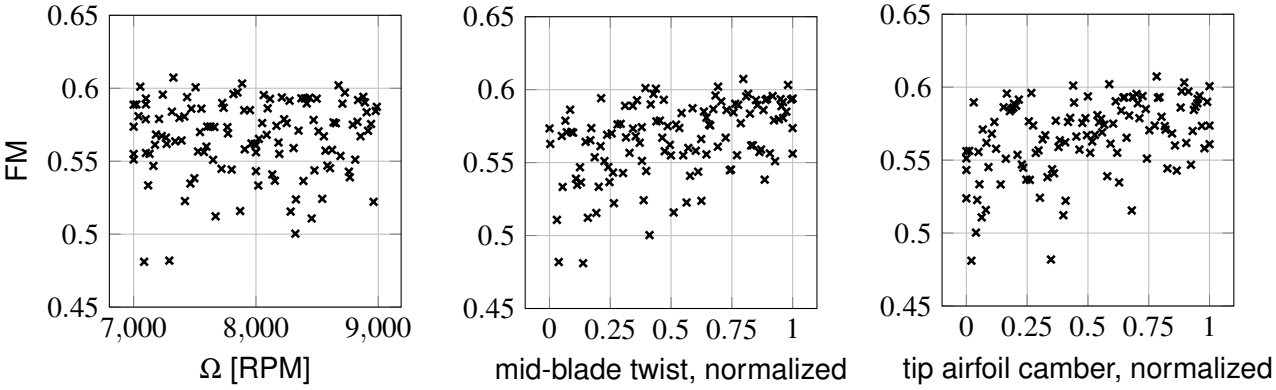


Figure 7 – FM plotted against selected input parameters: rotational speed (left), mid-blade twist (middle) and tip airfoil camber (right).

The number of plots required to perform one-by-one analysis of input-output relations grows rapidly with increasing number of variables and outputs. Therefore, a more compact way of visualizing parameter sensitivity is performed. Sobol' indices based analysis in Figure 8 shows the relative importance of individual parameters on the set of output parameters. It allows to quickly determine the unimportant parameters (all-blue columns) as well as the critical ones (yellow-red columns). In the current example, parameters 0, 3 and 8 do not have any meaningful influence on any output. On the other hand, parameters 10, 11 as well as 5, 6 and 7 capture majority of the variation of all outputs. The output-centered analysis is also simplified with this approach. For example, FM depends mainly on parameters 4-7 and 9-10, which describe blade twist and airfoil camber. The broadband component of SPL is almost entirely determined by parameters 10 and 11, which determine the tip airfoil camber and rotational speed. This observation is expected, as the parameters which influence trailing edge noise in the BPM model are freestream velocity and boundary layer properties, which in turn are directly controlled by the airfoil camber.

An additional analysis can be performed to determine the correlation between outputs. Figure 9 presents the tonal and broadband SPL correlation with thrust and FM. The tonal SPL component

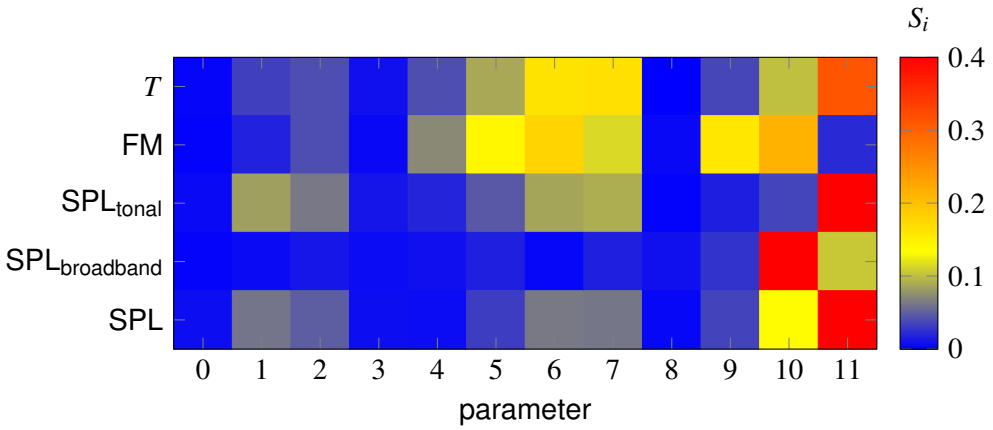


Figure 8 – First order Sobol' indices calculated based on the surrogate models of thrust, figure of merit and sound pressure levels.

correlates with thrust very well. Moreover, the highest FM for given thrust minimizes the tonal SPL, i.e. the optimization is expected to lead to similar results. On the other hand, the broadband SPL does not correlate with thrust and FM.

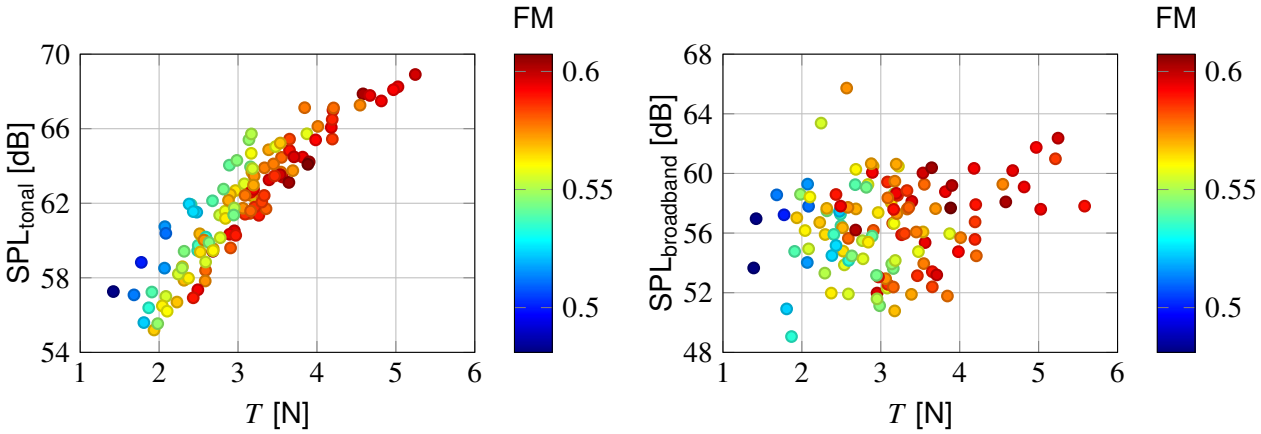


Figure 9 – Tonal (left) and broadband (right) SPL correlation with thrust and FM.

3.2.2 Optimization results

Result of the optimization process are in the form of a 4-dimensional Pareto front. Figure 10 presents three selected plots depicting the Pareto front obtained for each thrust constraint. It can be observed, that the blade generating lower thrust gives lower SPL only if FM is sacrificed. If relatively high FM is required, SPL is very similar, regardless of the thrust. The second plot, where the tonal component is plotted against FM explains that this behavior is due to the tonal component. The last plot presents the Pareto front on the tonal and broadband SPL axes. From the raw SPL minimization point of view, the designer is only interested in the minimization of the tonal component. The lowest tonal SPL is higher than the highest broadband SPL.

3.2.3 Concluding remarks

A comparison of A-weighted SPL is presented in Figure 11, depicting the importance of the objective function definition on the results. The tonal component of SPL is significantly reduced when A-weighting is applied. This is visualized using shaded regions and the red line marking the SPL=SPL_A boundary. On the other hand, the broadband SPL is affected relatively mildly. For lower values of the broadband SPL, the A-weighting reduces SPL, while for higher values SPL_A can be higher than SPL. It can be noted, that the magnitudes of broadband and tonal SPL_A are similar. Therefore, the selection of SPL_A as an objective function may lead to a different solution than the use of SPL. This

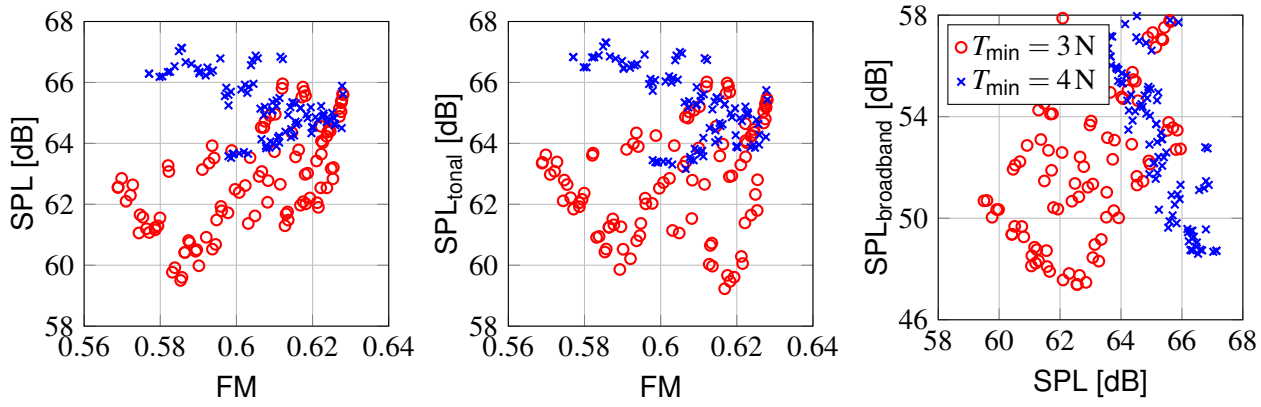


Figure 10 – Pareto fronts: FM-SPL (left), FM-SPL$_{tonal}$ (middle) and SPL-SPL$_{broadband}$ (right).

shows that the selection of a noise metric used in the optimization process is crucial. The challenge of defining a universal metric is currently a subject of research in various organizations.

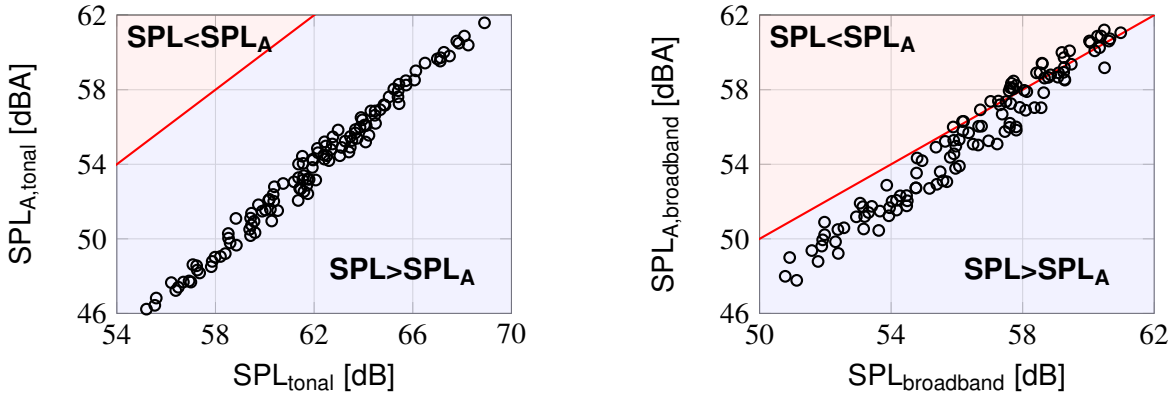


Figure 11 – Comparison of A-weighting on the tonal (left) and broadband (right) SPL.

Figure 12 presents 3-dimensional Pareto fronts resulting from the minimization of -FM, SPL, and SPL$_A$ for two values of required thrust. The front shapes for the FM-SPL and FM-SPL$_A$ highlight the influence of the required thrust. For the lower thrust constraint, the front spans over 6 dB or 8 dBA, whereas for the 4 N thrust constraint the front spans 2 dB or 5 dBA. An interesting feature was captured in the last plot, showing the Pareto front on the SPL-SPL$_A$ axes. For the lower thrust requirement the front converges to a very narrow area (left bottom of the plot), whereas for the higher thrust a steep front is formed. It depicts significantly higher sensitivity of the A-weighted SPL compared to SPL.

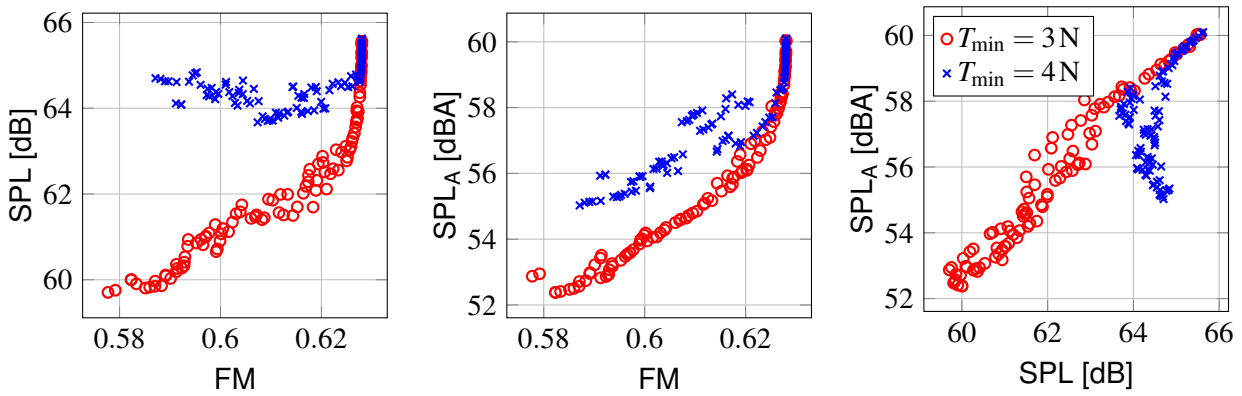


Figure 12 – Pareto fronts: FM-SPL (left), FM-SPL$_A$ (middle) and SPL-SPL$_A$ (right).

3.3 Multi-fidelity UAM rotor design

A UAM-class prop-rotor design is a prime example of a multi-point optimization problem. Table 1 presents operating conditions for hover and cruise—two essential flight phases of an eVTOL aircraft. This process was inspired by Joby Aviation S4, and uses its approximate specifications to define the optimization problem [15, 16, 17]. The required thrust in hover results from the weight of the aircraft and number of rotors, whereas the thrust in cruise was assumed based on a conservative lift-to-drag ratio of 10. Rotor rotating speeds in both phases were taken from the literature. The rotor has 5 blades and its radius was set to 1.5 m.

Table 1 – Multi-point specification.

flight phase	V [m/s]	Ω [RPM]	T_{req} [N]	$Q_{\max}$ [Nm]
hover	0	700	3000	700
cruise	40	650	300	700

The parametric model of the UAM propeller blade was defined with 4-knot splines defining chord and twist radial distributions, and 2 parameters defining the airfoil camber at the root and tip. The collective pitch required for effective transition between 2 distinct flight phases was included in the definition of lower and upper bounds of the twist-spline knots position. In summary, the parametric model consisted of 10 parameters.
The multi-point, multi-objective optimization problem takes the following form:

$$\begin{aligned} \underset{\mathbf{x}}{\text{minimize}} \quad & P_h(\mathbf{x}), P_c(\mathbf{x}), \text{SPL}_h(\mathbf{x}), \text{SPL}_c(\mathbf{x}) \\ \text{subject to} \quad & 3000 - T_h \leq 0, \\ & 300 - T_c \leq 0, \\ & \mathbf{l} \leq \mathbf{x} \leq \mathbf{u} \end{aligned}$$

with the maximum torque constraint dropped for clarity due to the use of the fixed rotational rate.
In this study, a multi-fidelity surrogate-based optimization process was used. Blade-resolved RANS and BEMT simulations were used respectively for higher (HF) and lower (LF) fidelity models. The initial nested sampling plan was generated with 60 HF and 240 LF points. Figure 13 presents correlations of thrust, torque and FM between samples. It can be observed that the models correlate very well in thrust, relatively well in torque and very poor in FM. Linear fit presented in plots shows that BEMT predicts lower torque and as a result—substantially higher figure of merit. The use of LF model was deemed useful in terms of thrust prediction, important to satisfy constraints.
The optimization process was carried out according to the standard surrogate-based optimization framework, with the use of multi-fidelity surrogate modeling. The example result of a propeller blade satisfying thrust constraints is presented in Figure 14, which depicts the effect of collective pitch, and in Figure 15, which presents pressure distributions on the blade surface in hover and cruise. It can be observed, that hover requires significantly lower pressure values on the top surface compared to cruise.
Figure 16 presents set of Pareto solutions on 4 plots. To simplify analysis of results, k-means clustering algorithm was used to automatically divide results based on their performance. For example, the blue cluster optimizes cruise and gives the highest SPL in hover. The red cluster gives the lowest power in hover, however, to obtain lower SPL the design from green or cyan cluster should be selected. The green cluster covers a large part of hover Pareto set, but it is the worst set for cruise. The multi-point, multi-objective analysis of results reveals significant trade-offs in realistic AAM prop-rotor design.
The mean radial distributions of chord and twist for each of 4 clusters are presented in Figure 17. It can be observed, that the cyan and green clusters have higher chords in the inboard part of the blade. These two groups minimize SPL in hover. The highest twist is observed in the blue and cyan groups—these groups minimize power in cruise. Figure 18 presents CAD models of two blades, marked with X in Figure 16. Hover optimum belongs to the green cluster, whereas power optimum belongs to the blue one.

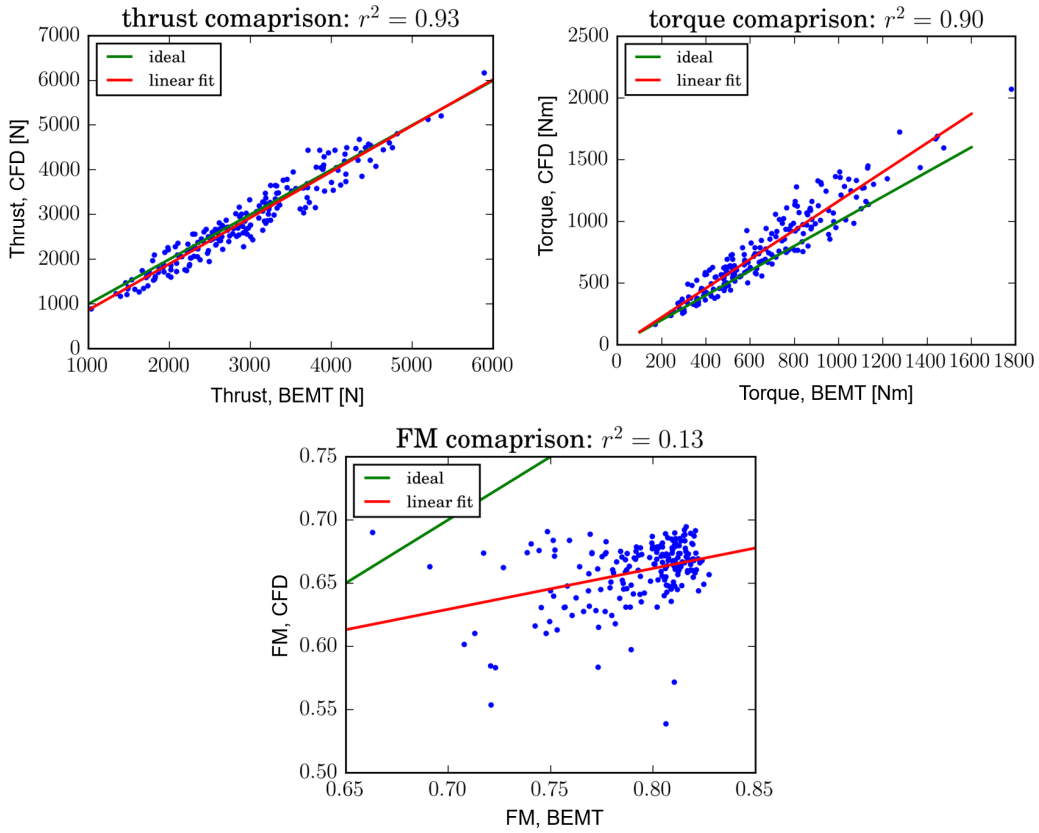


Figure 13 – Correlation between the LF and HF models for initial sample: thrust (left), torque (middle) and figure of merit (right).

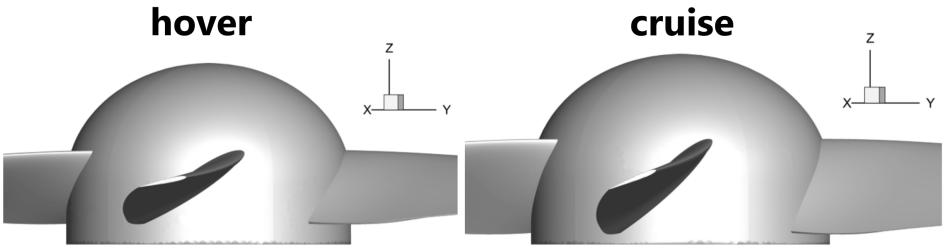


Figure 14 – Example of blade pitch change between hover (left) and cruise (right) phases.

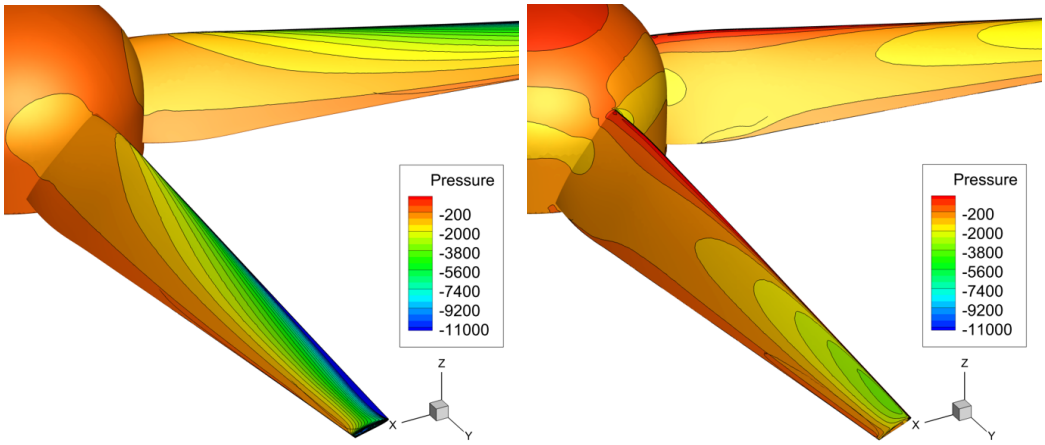


Figure 15 – Pressure (in Pascals) on the blade surface in hover (left) and cruise (right) phases.

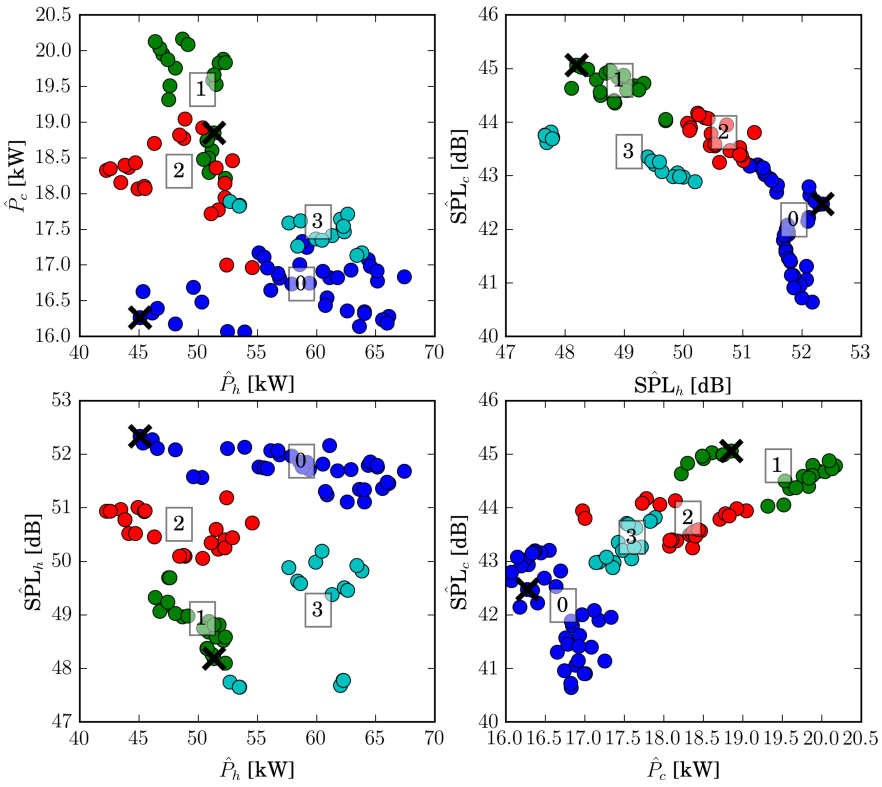


Figure 16 – Pareto fronts.

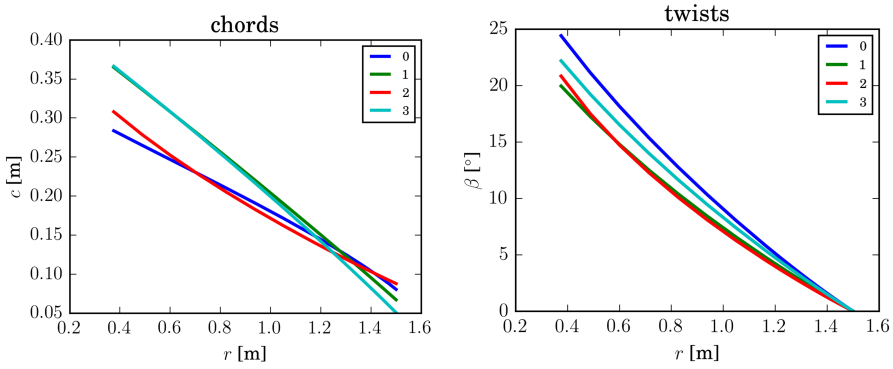


Figure 17 – Mean chord (left) and twist (right) distributions for each solution cluster.

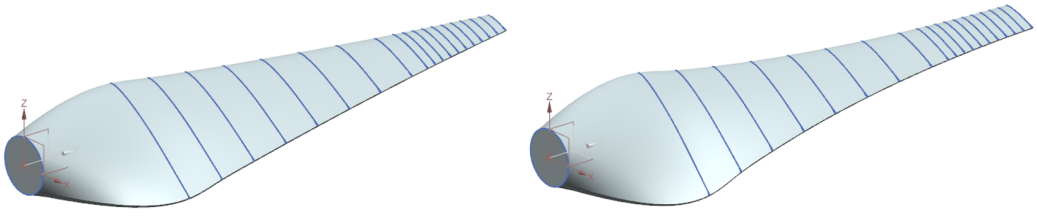


Figure 18 – Hover optimum (left) and power optimum (right).

The effectiveness of multi-fidelity approach was confirmed by comparing the prediction mean standard error and mean average error of multi-fidelity and high-fidelity-only surrogate models. The test involved cross-validation using 10% of the sample, with error metrics determined as an average of 30 evaluations performed for randomly selected sets of validation points. Both error metrics were significantly lower in multi-fidelity prediction for all modeled quantities, i.e. thrust, power and SPL. Moreover, the surrogates prediction was more accurate in the cruise phase. This is a consequence

of a better accuracy of BEMT for non-zero advance ratio.

4. Summary

This work presents the findings collected during the aeroacoustic design of rotors. The work focuses primarily on selecting suitable computational codes and design frameworks, and discusses various aspects of the optimization process. It investigates practical optimization problems, particularly those involving multiple operating points, objectives and disciplines. The main objective of this work is to draw readers' attention to several aspects that are not commonly discussed in the literature. The key aspects raised in the work and presented in case studies are:

- Selecting a blade parametric model, defining parameter bounds, and analyzing variance are all crucial steps in developing an efficient optimization process. While increasing the number of variables increases the cost of optimization, it may also result in a superior outcome. Defining the relative importance of design variables helps create an efficient optimization process. A parametric model inspired by the literature was established in the small-scale rotor design. The study showed negligible importance of several parameters defining the chord and twist distributions of a blade. Therefore, the parametric model can be improved by dropping these variables, or redefining their bounds to make the optimization process more efficient.
- The selection of objective functions for aeroacoustic optimization is crucial for determining the direction of optimization. The small-scale rotor design case study revealed significant differences when comparing two commonly used objective functions: A-weighted and unweighted SPL. There are a number of ways to determine the acoustic objective function (which are not limited to the selection of the weighting function). It is crucial to understand and define the optimization goal accordingly.
- Extending a single-fidelity optimization process to a multi-fidelity process can significantly improve cost efficiency. Even inexpensive models used for low-fidelity sampling can substantially improve the accuracy of surrogate models, as was presented in the UAM-class rotor design case study.

Contact Author Email Address

witold.klimczyk@ilot.lukasiewicz.gov.pl

Acknowledgments

This research was supported by CI TASK, Gdańsk, Poland.

Copyright Statement

The authors confirm that they, and/or their company or organization, hold copyright on all of the original material included in this paper. The authors also confirm that they have obtained permission, from the copyright holder of any third party material included in this paper, to publish it as part of their paper. The authors confirm that they give permission, or have obtained permission from the copyright holder of this paper, for the publication and distribution of this paper as part of the ICAS proceedings or as individual off-prints from the proceedings.

References

[1] Johnson W and Silva C. Nasa concept vehicles and the engineering of advanced air mobility aircraft. *The Aeronautical Journal*, 126(1295):59–91, 2022.

[2] Rizzi SA, Huff DL, Boyd DD, Bent P, Henderson BS, Pascioni KA, Sargent DC, Josephson DL, Marsan M, He HB, et al. Urban air mobility noise: Current practice, gaps, and recommendations. Technical report, 2020.

[3] Pietro Li Volsi, David Gomez-Ariza, Romain Gojon, Thierry Jardin, and Jean-Marc Moschetta. Aeroacoustic optimization of mav rotors. *International Journal of Micro Air Vehicles*, 14:17568293211070827, 2022.

[4] BU Yuepeng, Song Wenping, HAN Zhonghua, et al. Aerodynamic/aeroacoustic variable-fidelity optimization of helicopter rotor based on hierarchical kriging model. *Chinese Journal of Aeronautics*, 33(2):476–492, 2020.

[5] Matthew A Clarke and Emilio Botero. Aeroacoustic optimization of vtol rotor blades. In *AIAA SciTech 2023 Forum*, page 0209, 2023.

[6] Berk Sarikaya, Alessandro Zarri, Julien Christophe, Mohamed Hassanine Aissa, Tom Verstraete, and Christophe Schram. Aerodynamic and aeroacoustic design optimization of uavs using a surrogate model. *Journal of Sound and Vibration*, 589:118539, 2024.

[7] Daniel Ingraham, Justin S Gray, and Leonard V Lopes. Gradient-based propeller optimization with acoustic constraints. In *Aiaa scitech 2019 forum*, page 1219, 2019.

[8] Ohad Gur and Aviv Rosen. Optimization of propeller based propulsion system. *Journal of Aircraft*, 46(1):95–106, 2009.

[9] Klimczyk W. Aerodynamic design and optimization of propellers for multirotor. *Aircraft Engineering and Aerospace Technology*, 94(1):21–30, 2022.

[10] Klimczyk W and Sieradzki A. Rans-based aeroacoustic global sensitivity study and optimization of uav propellers. *Aerospace*, 10(3):306, 2023.

[11] Sieradzki A, Kekus-Kumor P, and Klimczyk W. Validation of a surrogate-based methodology for low-noise uav/uam rotor design. In *49th European Rotorcraft Forum 2023*, pages 1–13, 2023.

[12] Brentner KS and Farassat F. Modeling aerodynamically generated sound of helicopter rotors. *Progress in aerospace sciences*, 39(2-3):83–120, 2003.

[13] Thomas F Brooks, D Stuart Pope, and Michael A Marcolini. Airfoil self-noise and prediction. Technical report, 1989.

[14] Patrick Moriarty. Nafnoise user's guide. *National Wind Technology Center, National Renewable Energy Laboratory*, 2005.

[15] Jeremy Bain, Alex Stoll, and Gregor Mikic. Aerodynamic and acoustic design of the joby aviation evtol propeller. In *Proceedings of the Vertical Flight Society 77th Annual Forum*, pages 1–10. The Vertical Flight Society, 2021.

[16] Alex Stoll and Gregor Veble Mikić. Transition performance of tilt propeller aircraft. In *Vertical Flight Society 78th Annual Forum and Technology Display*. The Vertical Flight Society, 2022.

[17] Kyle A Pascioni, Michael E Watts, Mary Houston, Andrew Lind, James H Stephenson, and Jeremy Bain. Acoustic flight test of the joby aviation advanced air mobility prototype vehicle. In *28th AIAA/CEAS Aeroacoustics 2022 Conference*, page 3036, 2022.